A novel biopolymer for mucosal adjuvant against respiratory pathogens

Ashley R. Hoover[1,2]*, Sunil More[3]*, Kaili Liu[1], Connor L. West[1], Trisha I. Valero[1], Ningli Yu[1], Crystal Villalva[3], Amit Kumar[4], Lu Alleruzzo[5], Samuel S. K. Lam[5], Tomas Hode[5], James F. Papin[6], and Wei R. Chen[1,#]

[1] Stephenson School of Biomedical Engineering, University of Oklahoma, Norman, OK, USA

[2] Arthritis and Clinical Immunology Research Program, Oklahoma Medical Research Foundation, Oklahoma City, OK, USA

[3] Veterinary Pathobiology, College of Veterinary Medicine, Oklahoma State University, Stillwater, OK USA

[4] Labcorp Drug Development solutions or Labcorp Inc. 3301 Kindman Blvd. Madison, WI, USA

[5] Immunophotonics, Inc., 4340 Duncan Avenue, Suite 212, Saint Louis, MO, USA

[6] Department Pathology and Division of Comparative Medicine, University of Oklahoma Health Sciences Center, Oklahoma City, USA

* Authors contributed equally

Corresponding author: wei-r-chen@ou.edu

Abstract

Mucosal vaccinations for respiratory pathogens provide superior protection as they stimulate localized cellular and humoral immunity at the site of infection. Currently, the major limitation of the intranasal vaccination is using effective adjuvants capable of withstanding the harsh environment imposed by the mucosa. Herein, we describe the efficacy of using a novel biopolymer, N-dihydrogalactochitosan (GC), as a nasal mucosal vaccine adjuvant against respiratory infections. Specifically, using COVID as an example, we mixed GC with recombinant SARS-CoV-2 trimeric spike (S) and nucleocapsid (NC) proteins to intranasally vaccinate K18-hACE2 transgenic mice, in comparison with Addavax (AV), an MF-59 equivalent. In contrast to AV, intranasal application of GC induces a robust, systemic antigen-specific antibody response and increases the number of T cells in the cervical lymph nodes. Moreover, GC+S+NC vaccinated animals were largely resistant to lethal SARS-CoV-2 challenge and experienced drastically reduced morbidity and mortality, with the animal weights and behavior returning to normal 22 days post infection. In contrast, animals intranasally vaccinated by AV+S+NC experienced severe weight loss, mortality, and respiratory distress, with none surviving beyond 6 days post infection. Our findings demonstrate that GC can serve as a potent mucosal vaccine adjuvant against SARS-CoV-2 and potentially other respiratory viruses.

Keywords: N-dihydrogalactochitosan (GC), mucosal vaccine adjuvant, intranasal vaccination, recombinant viral proteins, respiratory infection

Introduction

Worldwide, respiratory tract infections are the most common type of infection found in both adults and children[1]. They manifest a variety of symptoms generally limited to the upper respiratory tract, but occasionally they can become more sinister and result in pneumonia, significant lung damage, and/or even death, predominantly in young children or elderly adults[2]. Successful respiratory viral vaccination requires the development of a broad repertoire of antibodies (humoral immunity, IgA and IgG), T Helper 1 (Th1, interferon gamma: IFNγ), and cytotoxic T cell responses (cellular immunity) systemically and specifically at the site of infection. Mucosal vaccination for respiratory viruses is an attractive option as it can trigger both humoral and cellular immunities locally and systemically[3, 4, 5].

The current intranasal vaccines approved for human use, such as FluMist and NASOVAC, employ live attenuated virus (LAV)[6]. LAVs are attractive because they generate broader, more robust, and durable immune responses against the targeted pathogen and possible variants[7]. Moreover, LAVs mimic natural infection and thus stimulate an effective immune response. Despite their effectiveness, there are drawbacks to LAVs. They are temperature sensitive and can regain virulence in some cases and are thus not recommended for individuals with severely compromised immune systems[8, 9, 10]. Additionally, during the attenuation process, the immunogenicity of the pathogen can become compromised, resulting in only moderate immune protection[6, 11]. Whole inactivated viruses and subunit vaccines do not have the issue of temperature sensitivity or the ability to regain virulence, but the immunogenicity of these vaccines can be compromised[10, 12, 13]. To increase the immunogenicity of inactivated virus and subunit vaccines, adjuvants are needed to enhance the cellular and/or humoral immune response to the targeted pathogens[14, 15].

Development of adjuvants for mucosal vaccines faces significant challenges due to the nature of the mucosa, which contains several components that provide a protective barrier between the outside environment and our internal organ systems. It consists of a single epithelial layer that is covered with protective mucus, antimicrobial proteins, and symbiotic microbiota that maintain a low pH value[16, 17]. The epithelial layer is peppered with intraepithelial tissue resident innate and adaptive immune cells, and specialized mucosal

associated lymphoid structures capable of responding to pathogen invasion[16, 17]. Thus, an ideal mucosal adjuvant must be able to withstand the harsh environment of the mucosal surface, maintain the antigen at the site of inoculation for an extended period, activate/recruit immune cells to the site of administration, and stimulate an immune response like the naturally infecting pathogens. For respiratory viral pathogens, the ideal adjuvant needs to drive a type I interferon response, since these cytokines play a critical role in initiating antiviral immunity and generating tissue resident immune cells in the respiratory epithelium[18, 19].

Using adjuvants, such as cyclic dinucleotides, which elicit the production of type I IFN through STING signaling, leads to enhanced humoral and cellular immunities capable of preventing and eliminating intracellular pathogen infections following vaccination[20, 21]. However, the cyclic dinucleotides must be administered repeatedly, in high quantities, and/or modified to prevent host cell inactivation[20, 21, 22].

To overcome these and other limitations of existing mucosal adjuvants, we developed N-dihydrogalactochitosan (GC), a new molecule that is synthesized from galactose and chitosan[23]. Compared to the immune responses induced by its chitosan precursor[24, 25], GC exhibits superior potency in inducing the type I IFN pathway[26]. In addition, GC has improved solubility over chitosan, and retains many of the favorable properties of chitosan, including its low toxicity, biodegradability, low-pH resistance, biocompatibility, and mucoadhesive nature.

Chitosan is currently used in a variety of chemical, agricultural, pharmacological, and medicinal applications[27, 28]. However, its poor solubility, high potential to be contaminated with endotoxins, and poor characterization of the polymeric mixture, has limited its uses as a commercial medicinal product[29]. GC has been synthesized and purified under GMP conditions, with comprehensive structural characterization, extensive testing for metals, endotoxins and other impurities, and with superior potency and improved solubility over its corresponding chitosan starting material, further addressing the major challenges in applications of chitosan. GC is currently developed as a medicinal product (referred to as IP-001) as a multi-modal immune stimulant to generate a systemic antitumor immune response when administered in conjunction with tumor ablation[30, 31, 32].

In the present work, GC was used as a mucosal adjuvant for intranasal vaccines due to its functions as an immunostimulant/adjuvant. To mitigate the drawbacks of live attenuated virus as mentioned, we used recombinant SARS-CoV-2 trimeric spike (S) and nucleocapsid (NC) proteins with GC for nasal vaccine formulation. K18-hACE2 mice were immunized intranasally with GC+NC+S and compared with Addavax (AV), an MF-59 equivalent. We found that GC produces a robust, systemic antigen-specific antibody response and increases the number of T cells in the cervical lymph nodes following intranasal vaccination to a greater degree than AV. More importantly, animals vaccinated with GC+S+NC were strongly resistant to lethal SARS-CoV-2 viral challenge and experienced drastically reduced weight loss and mortality, with complete recovery 22 days post infection. In contrast, AV+S+NC vaccinated animals all succumbed to infection within 6 days of the SARS-CoV-2 viral challenge, while experiencing severe weight loss, mortality, and respiratory distress. Our findings make a strong case for using GC as a mucosal adjuvant for intranasal vaccine. Not only does GC alone drive an antiviral response in antigen presenting cells (APCs), but also simply combing it with recombinant proteins creates a highly effective mucosal vaccine against coronaviruses.

Results

GC retains antigen at the administration site and activates a variety of pattern recognition receptors (PRRs) involved in viral responses

Since one of the important functions of an effective vaccine adjuvant is to retain the antigens, we examined GC's ability to retain ovalbumin labeled with Texas-Red (OVA-TR). We mixed GC of different concentrations (0.5, 0.75, 0.9, or 1%) with OVA-TR and injected the mixture subcutaneously in the flank of C57BL/6 mice, followed with whole body fluorescent imaging over a period of seven days (Supplemental Figure 1A). We observed that GC at a higher concentration (0.9 and 1.0%) was able to retain OVA at the administration site significantly longer than PBS (Figure 1A, Supplemental Figure 1B). Specifically, ~50% of the OVA was retained at the administration site by the 1% GC solution 3 days post injection (Figure 1A).

Furthermore, when GC alone was delivered intranasally, at a concentration of 0.75%, the total $CD45^+$ cellularity and B cell cellularity in the cervical lymph nodes (cLNs) were significantly increased 72 hours post

inoculation (Supplemental Figure 1C). In addition, we observed a trending increase in the number of migrating and resident DCs, and $CD4^+$ and $CD8^+$ T cells in the cLNs (Supplemental Figure 1C). These data suggest that GC can induce a local response, leading to the migration and activation of lymphocytes in the nasal-associated lymphoid tissue (NALT).

To determine the regulation of gene expression in bone marrow derived dendritic cells (BMDCs) by GC, we performed bulk RNA-sequencing analysis of GC-stimulated BMDCs. Our results revealed that a variety of gene expression pathways involved in anti-viral responses, including responses against Covid-19, were highly enriched in GC stimulated BMDCs (Figure 1B). Several pathways involved in antigen processing and presentation, cytokine-cytokine receptor signaling, cell adhesion, cell-cell interaction, and antibody production networks, were also upregulated (Supplemental Figure 1D). Moreover, a variety of pattern recognition receptors (PRRs), most notably a diverse array of nucleic acid PRRs, including *Cgas, Zbp1, Tlr3, Tlr7, Tlr9, Mavs,* and *Ifih1,* were activated in BMDCs in response to GC (Figure 1C). Taken together, these results suggest that GC acts as a potent adjuvant for recombinant protein vaccination as it activates multiple PRRs, drives the expression of genes required for T cell activation and differentiation, and triggers a variety of viral response pathways required to initiate antiviral immunity.

GC drives strong antigen-specific humoral immune responses following a two-dose vaccine regimen

To examine the adjuvant function of GC in inducing humoral immune responses, we prepared a recombinant viral protein (RVPs)-based vaccine, by mixing 1% GC with 5μg of either recombinant SARS-CoV-2 trimeric spike (S) protein or the SARS-CoV-2 nucleocapsid (NC) protein. C57BL/6 mice (8 weeks old) were vaccinated intranasally (I.N.) once (1X) with GC, GC+S, and GC+NC. The serum, lungs, and the cLNs were collected for analysis two weeks later (Supplemental Figure 2A). Total serum IgG and IgA were unchanged amongst all the vaccinated groups (Supplemental Figure 2B) and S-specific antibodies were not detected at this time point (data not shown). Lung cellularity and IgA levels were also unchanged in all the groups (data not shown). In the cLNs, total $CD8^+$ T cells and naïve $CD8^+CD62L^+$ T cells were increased in the GC+NC 1X vaccinated animals compared to PBS or GC groups (Supplemental Figure 2C). For $CD4^+$ T cells, the memory $CD44^+CD62L^+$ $CD4^+$

T cells were significantly increased after GC+NC vaccination compared to PBS controls (Supplemental Figure 2D), and B cell numbers were largely unchanged (Supplemental Figure 2E). While 1X vaccination was able to increase lymph node cellularity (Supplemental Figure 2C), it was unable to generate S-specific antibodies at a detectable concentration (data not shown). This suggests that one I.N. vaccination may not be sufficient to induce significant immune responses against viral infection.

We next vaccinated mice with S protein I.N. twice (2X), four weeks apart, and examined the humoral and cellular immune responses at different time points after vaccination (Figure 2A). We also used the MF-59 equivalent, Addavax (AV), as a comparing adjuvant, because MF-59 is currently used in human vaccines against viral infections (including influenza) and it has been demonstrated to enhance the mucosal immunogenicity of recombinant protein vaccination[14, 33]. PBS, 1% GC, or AV (15μl) was mixed with 2.5μg S protein and used for the two-dose vaccination scheme. Two weeks after the 2nd vaccination, left lung lobe homogenates were acquired and total IgA and S-specific IgA were measured via antibody ELISA (Figure 2B). While not significant by One-Way ANOVA, total IgA in both GC+S and AV+S vaccinated animals was trending higher than PBS controls. Only S-specific IgA was significantly higher in the GC+S vaccinated animals compared to PBS controls (Figure 2B). Total serum IgG1 and IgG2c antibodies were measured one week after the 1st vaccination, one week after the 2nd vaccination, and two weeks after the 2nd vaccination (Figure 2C-D). One week after either the 1st vaccination or the 2nd vaccination, there were no significant differences in total IgG1 among the four groups (Figure 2C). Two weeks after the 2nd vaccination, total IgG1 in both GC+S and AV+S groups was trending up but not significantly by One-Way ANOVA (Figure 2C). Interestingly, S-specific antibodies were not detected in the PBS samples but was observed in both AV+S and GC+S vaccinated animals (Figure 2C). While IgG2c showed little change one week after first vaccination, it is trending up in PBS+S, GC+S, and AV+S vaccinated animals one week after second vaccination (Figure 2D). Interestingly, two weeks after the 2nd vaccination IgG2c levels returned to the levels observed one week after the first vaccination (Figure 2D). Mirroring what was observed with S-specific IgG1 (Figure 2C), S-specific IgG2c was only represented in the AV+S and GC+S vaccinated group, suggesting that GC drives a similar systemic antigen specific antibody response to AV+S vaccination (Figure 2D). Taken together, these data

indicate that GC induces a satisfactory antigen-specific humoral immune response that is comparable and possibly superior to a known vaccine adjuvant, AV, when delivered mucosally.

GC drives strong cellular responses following a two-dose vaccination regimen

In addition to the humoral immune responses, we examined the numbers of T and B cells residing within the cLN and the lungs following the same vaccination schedule described in Figure 2A. While not significant by one-way ANOVA, there was a trending increase in the total $CD8^+$ T cells and specific $CD8^+$ T cell subsets in the cLN of GC+S or AV+S vaccinated animals (Figure 3A). Interestingly, GC+S vaccinated animals experienced a trending increase in $CD8^+CD44^+CD62L^+$ and $CD8^+CD62L^+$ T cells while AV+S vaccinated animals demonstrated a trending increase in $CD8^+CD44^+$ and $CD8^+CD62L^+$ T cells (Figure 3A). In contrast, $CD4^+CD44^+$ and $CD4^+CD44^+CD62L^+$ were both significantly increased in the cLN of GC+S vaccinated animals but not in AV+S vaccinated animals (Figure 3B). B cells were not significantly affected in all experimental groups (Figure 3C).

Next, we examined the lung cellularity following the two-dose vaccine regimen. GC+S vaccinated animals did not experience an increase of $CD8^+$ T cells, $CD4^+$ T cells, or B cells (Supplemental Figure 3 A-C). However, AV+S vaccinated animals appeared to have a trending increase in $CD8^+$ T cells and $CD8^+$ T cell subsets (Supplemental Figure 3A). Total $CD4^+$ T cells were trending up in AV+S vaccinated animals, but this was not reflected in the three $CD4^+$ T cell subsets examined (Supplemental Figure 3B). Furthermore, B cells numbers also had a trending increase in AV+S vaccinated animals, which was not observed in the other 3 groups. Overall, the T cell cellularity within the lung following a two-dose I.N. vaccination regimen resulted in minimal changes.

Combining GC with the trimeric spike protein and the nucleocapsid protein increases the influx of T cells into the lung following intranasal vaccination

Next, to increase the cellular response in the lung following vaccination and to increase the coverage of antigens, we examined the combined effects of NC protein + S protein, as the NC protein is one of the most abundant proteins in SARS-CoV-2 infected patients and it protects the viral RNA. To examine whether the

addition of the NC protein could increase the robustness of recombinant protein vaccine responses, we vaccinated animals 2X, 4 weeks apart, with either GC+5μg S, GC+5μg NC, or GC+ 2.5μg S + 2.5μg NC. Two weeks after the 2nd vaccination, the serum, lungs, and cLNs were examined for antibody and cellular responses. In the serum we found that the total IgG1 and IgG2c antibodies levels were largely unchanged in the GC+S, GC+NC, or GC+S+NC vaccinated animals compared to the PBS controls (Figure 4A-B). However, when examining S-specific IgG1 and IgG2c we found that GC+S+NC, with reduced dose of S and NC proteins (2.5μg), made equivalent S-specific IgG1 and IgG2c compared to GC with higher dose of S protein (5μg) (Figure 4A-B). A similar trend was observed in the lungs with total IgA and S-specific IgA (Figure 4C), with GC+S+NC producing significantly more S-specific IgA than the PBS alone or GC+NC vaccinated animals.

In the cLNs of the GC+S, GC+NC, or GC+S+NC vaccinated animals, trending increases in total and $CD4^+$ and $CD8^+$ T cell subsets (Figure 4D-E) were observed, with only the $CD4^+CD44^+$ T cells being significantly increased in GC+S+NC vaccinated animals (Figure 4D). In the lungs, using either 5μg S protein or 5μg NC protein, instead of using 2.5μg S which was used for the experiments shown in Figures 2 and 3, resulted in a trending increase in total $CD4^+$ and $CD8^+$ T cells and their subsets and B cells (Supplemental Figure 4A-C). Combining 2.5μg S and 2.5μg NC proteins with GC resulted in an equivalent trending increase, suggesting that S and NC proteins are synergistic and can generate more diverse immune response because it is targeting two separate SARS-CoV-2 proteins. For this reason, we chose to use the S+NC combination for viral challenge.

Animals vaccinated by trimeric spike and nucleocapsid proteins + GC are resistant to lethal SARS-CoV-2 viral challenge

For viral challenge experiments, we vaccinated C57BL/6 transgenic mice expressing the human angiotensin 1-converting enzyme 2 (ACE2) receptor under control of the cytokeratin-18 (K18) gene promotor (K18-hACE2 mice). K18-hACE2 mice were vaccinated using the two-dose regimen described in the Figure 2A. Six weeks after the 2nd vaccination, animals were challenged with a lethal dose of SARS-CoV-2 and monitored for 21 days (Figure 5A). Efficacy following virus challenge was compared for six vaccine combinations: PBS, PBS+S+NC,

GC, GC+S+NC, AV, or AV+S+NC. Within the first seven days following the lethal viral challenge, all mice in the PBS, and the GC vaccinated groups either died or were humanely euthanized due to severe clinical signs or weight loss (Figure 5B-C). One of six animals in the AV group survived, while two of ten PBS+S+NC vaccinated animals survived. Unexpectedly, all nine AV+S+NC vaccinated animals either died or had to be humanely euthanized (Figure 5B-C). Excitingly, in the GC+S+NC vaccinated group, 13 of the 15 vaccinated animals experienced minimal weight loss on 1st and 2nd day post infection and survived without obvious complications (Figure 5B-C). Only two animals in the GC+S+NC group experienced weight loss and died within eight days of viral challenge.

As an alternative measure of vaccine efficacy to complement survival outcomes, we analyzed their viral loads in the lungs following infection. Five days post viral infection, three mice were randomly selected from each of the six groups and lung viral titers were assessed via plaque assays (Figure 5D). The mice in GC alone and AV+S+NC groups exhibited higher virus titers than that in the other groups, but the titers were not statistically significant with the number of animals used. Interestingly, only one mouse in the GC+S+NC group generated viral plaques, suggesting that GC+S+NC either mitigates virus replication in the lungs or reduces the amount of virus entering and infecting the lungs.

GC + trimeric spike and nucleocapsid proteins protected animals from lung pathology following SARS-CoV-2 viral infection

The histopathology of the lungs from the six groups of vaccinated animals was analyzed at multiple timepoints post-infection. Prominent histopathology features were interstitial pneumonia, infiltration of inflammatory cells (lymphocytes, neutrophils, and macrophages), and bronchiectasia. The histology of the lungs and the pathology scores at day 0 are shown in Figure 6A and 6E. All the groups exhibited comparative pathology scores at day 3 (Figure 6B and 6F) when comparing a variety of lung pathology parameters. The most prominent features on day 3 were peribronchial and perivascular infiltration of lymphocytes (Figure 6B, empty circles). The interstitium was thickened and expanded with low numbers of lymphocytes, macrophages, and neutrophils (Figure 5B, arrow). On days 5 and 6 post-infection, the PBS, GC, and PBS+S+NC groups exhibited the most

severe changes (Figure 6C and 6G-H). Bronchiectasia was evident on day 6 in the PBS, AV, and GC groups (Figure 6C, arrowhead). The bronchioles were infiltrated and expanded with moderate to large amounts of mucus admixed with inflammatory cells (bronchiectasia, Figure 6C, black arrows) in groups PBS+S+NC, AV+S+NC, and GC+S+NC. There were also moderate numbers of lymphocytes, neutrophils, and macrophages in the interstitium (Figure 6C, arrow) and extending into the alveoli (Figure 6C, empty arrowhead) in the three S+NC groups. In addition, the GC group exhibited moderate hemorrhages in the alveolar spaces (Fig. 6C; *). While the lungs of GC+S+NC vaccinated exhibited peribronchiolar and perivascular inflammation six days after viral challenge, there was a complete absence of bronchiectasia (Figure 6C). While the lungs of GC+S+NC vaccinated animals exhibited pathologic lesions, they were mild and were not to the level or severity experienced with the other groups. A mouse in the GC+S+NC vaccinated group (Figure 6H) was sick and received high pathology scores but this was likely stochastic as survival rate in this group was significant higher compared to the other groups. Lung pathology analysis 21 days post infection revealed a significant reduction in the lung pathology in the GC+S+NC vaccinated animals (Figure 6D and 6I). The GC+S+NC animals had characteristics of open alveolar spaces, low amounts of perivascular and peribronchiolar cuffing as compared to AV and PBS+S+NC at day 21 (Figure 6D and 6I).

Discussion

Mucosal vaccination has the ability to induce local and systemic humoral and cellular immunities[3, 4, 5] and mucosal adjuvants are critical to developing effective vaccines against respiratory viruses[34]. Key characteristics of successful vaccine adjuvants are their ability to enhance the immunogenicity of an antigen via retention and slow release, enhance the phagocytic capability of APCs, and reduce the amount of antigen required to stimulate protective immune responses[35]. This is reflected in their ability to boost humoral responses with antibody production and cellular responses through memory T cell formation. Moreover, vaccine adjuvants should drive an immune response similar to immune responses generated by the specific pathogen. Hence a type I IFN response would be ideal for respiratory virus as type I IFNs are required for antiviral immunity[36, 37,

[38]. Thus far, most adjuvants currently used for human vaccines have been unable to activate a multitude of PRRs simultaneously; only one adjuvant, cytosine phosphoguanosine 1018 (CpG 1018), a TLR9 agonist, stimulates the production of type I IFN[14, 39, 40]. We developed N-dihydrogalactochitosan (GC), a novel biopolymer, as an effective mucosal vaccine adjuvant. In this study, we demonstrated GC's adjuvant functions in a recombinant viral protein-based vaccine against respiratory pathogens, using SARS-CoV-2 as an example. Because of its physical and chemical properties, GC poses strong retention power in retaining antigens at the administration site at an appropriate concentration, as shown in Figure 1A and Supplemental Figure 1B. Furthermore, GC activated several different nucleic acid PRRs (Figure 1C), all of which were downstream of STING signaling and led to type I IFN and IL-1β production[26]. GC also activated immune pathways involved in response to Covid-19, as shown in Figure 1B.

In our previous work, we discovered that GC was able to produce a strong type I IFN response in tumor-infiltrating leukocytes (TILs) following its direct injection into the tumor[31, 41]. However, we also found that GC did not cause direct, non-specific activation of T cells, but instead works through the activation the APCs (data not shown). To determine the critical roles of dendritic cells (DCs) in antigen presentation, T cell activation and differentiation, and effector and memory T cell formation, we discovered the pathways of T cell activation through DC activation, consistent with previous published results[42, 43]. We have previously shown that GC directly induces maturation of dendritic cells via increased co-stimulatory molecules CD80, CD40 and MHC-II[44]. Similarly, activation of DCs by GC was also observed using mouse DC cell line DC2.4[45] or DCs isolated from a GC-injected tumor and tumor draining lymph node[44]. In a follow-up study using murine BMDCs, it was found that GC activates DCs in part via STING signaling leading to IFNβ/α (type I IFNs) and IL-1β production[42].

We demonstrated that GC was also capable of activating multiple PRRs to induce the production of type I IFN and IL-1β, including nucleic acid sensing pathways that play a significant role in antiviral immunity (Figure 1C). Type I IFNs have been shown to provide a "third signal" to T cells responding to a presented antigen, enhancing their effector function and clonal expansion[46]. IL-1β enhances the expansion, differentiation, memory formation, and migration of antigen-primed $CD4^+$ and $CD8^+$ T cells [47]. Moreover, the addition of IL-1β

enhances the efficacy of weakly immunogenic vaccines[47]. We found that GC+S vaccination could recruit T cells into the axillary lymph nodes to a greater extent than AV+S (Figure 3). Furthermore, GC vaccination was able to significantly increase the cellularity of $CD4^+$ T cells in the cervical lymph nodes, but with the S protein alone, no changes were observed in the lung (Figure 3).

NC protein is highly immunogenic, highly conserved with a much slower mutation rate than the S protein, and it drives robust T and B cell responses[48, 49, 50, 51]. Therefore, to further enhance the influx of immune cells into the lung following intranasal vaccination, we combined the S protein with the NC protein. GC+S+NC generated S-specific antibody responses in the lung and serum after two vaccinations (Figure 4A-C). More importantly, GC+S+NC increased the cellularity of T cells in the cervical lymph nodes and resulted in a trending increase of T and B cells within the lungs of the twice vaccinated animals (Figure 4, Supplemental Figure 4). These results prompted us to vaccinate K18-hACE2 transgenic mice using S+NC mixed with either PBS, AV, or GC, followed by SARS-CoV-2 viral challenge of a lethal dose.

Six weeks after the second vaccination K18-hACE2 transgenic mice were intranasally challenged with SARS-CoV-2 virus. GC+S+NC vaccination potently prevented robust infection, morbidity (clinical signs and weight loss), and mortality, and exhibited significantly reduced viral load, and severe lung pathology, in response to SARS-CoV-2 viral challenge (Figures 5 and 6). Surprisingly, AV+S+NC vaccination neither prevented mortality, nor reduced viral load, lung pathology, or weight loss. In fact, this group of animals performed significantly worse than all four control groups: PBS, GC, AV, PBS+S+NC, as shown in Figure 5. Lung pathology revealed that the AV+S+NC vaccinated animals experienced severe bronchiectasia and interstitial inflammation 3- and 6-days post infection (Figure 6B-C). This result was unexpected as the AV+S vaccinated animals generated a comparable humoral and cellular responses to GC+S in the lungs and cervical lymph nodes (Figures 2 and 3). These results suggest that only appropriate adjuvants should be used for lower respiratory tract infections, and that the wrong type of adjuvants can make the lung pathology significantly worse.

Bronchial changes such as bronchiectasia are detrimental to COVID-19 patients[52] as well as in a variety of other chronic lung diseases such as COPD[53] and can also be seen in patients in acute phase of SARS-CoV-2

infection[54]. We observed a tremendous increase in intraluminal bronchiolar mucus with inflammatory cells leading to expansion of the bronchioles in all the control groups (Figure 6B-D). Interestingly, GC+S+NC vaccinated mice did not exhibit this phenomenon, indicative of the lung protection by GC+S+NC against bronchiolar structural damage caused by the viral challenge (Figure 6B-D). Furthermore, the absence of bronchiectasia correlates well with the observation of the GC+S+NC vaccinated mice experiencing little to no respiratory distress. These animals were likely well ventilated, resulting in significantly reduced morbidity and mortality even though their cumulative histopathology scores were not significant lower.

In summary, the results presented herein reveal that GC acts as a potent mucosal vaccine adjuvant using recombinant viral proteins to prevent severe lung pathology and mortality in mice. GC's effectiveness as a viral vaccine adjuvant is likely due to the fact that it can retain the antigen in the mucosa for an extended period and it activates the same pathways involved in antiviral responses, thus driving potent antiviral immunity. Future work will focus on the understanding of GC's localized immune effect on the nasal mucosa, longevity of the immune response, and altering parameters of the vaccination to create the most effective intranasal immune response.

Materials and Methods

Animals: All animal studies were approved by the IACUC in Oklahoma Medical Research Foundation, the University of Oklahoma, and Oklahoma State University. C57BL/6 were purchased from Jackson Laboratories (Stock number: 000664). Wild type C57BL/6 mice were used for the studies to analyze the cellular and humoral response to vaccination using either GC (Immunophotonics, Inc., St. Louis, MO) and/or Addavax (InvivoGen, cat# vac-adx-10). B6.Cg-Tg(K18-ACE2)2Prlmn/J were purchased from Jackson Laboratories (Stock number: 034860)[55] and were used for vaccination and viral challenge with SARS-CoV-2 to test the efficacy of recombinant protein/adjuvant intranasal vaccination.

Antigen Retention by GC: Soluble OVA labeled with Texas-Red (OVA-TR) was purchased from Life Technologies/Invitrogen (5mg in lyophilized powder) and reconstituted with 1.25ml PBS to achieve a concentration of 4mg/ml. OVA-TR was further diluted with PBS to a concentration of 0.8mg/ml, and then

mixed 1:1 with 2% IP-001, or PBS as control, to achieve a final solution with 0.4mg/ml OVA-TR in 1% GC. GC+OVA-TR solutions were also prepared with different GC concentrations (0.9, 0.75, and 0.5%). Then GC+OVA-TR of 100ul volume was injected subcutaneously into the flank/back of shaved C57BL/6 mice. Whole body fluorescent imaging (IVIS 100) was performed over a period of several days. A region of interest ROI was drawn at the injection site for quantification of fluorescence from Texas red, which serves as the surrogate for the amount of OVA. The percentage change in fluorescence over time was calculated by comparison to the starting value taken shortly after injection. Two-way ANOVA was used for statistical analysis.

ELISA: Total IgA (Cat# 88-50450-88), IgG1 (Cat# 88-50410-86), and IgG2c (Cat# 88-50670-22) ELISA kits were purchased from ThermoFisher Scientific and were used according to manufactures instructions for the serum. Lung samples were diluted 1/1000 for analysis. For analysis of Trimeric Spike specific antibodies, Nunc MaxiSorp ELISA plates (Biolegend, Cat# 423501) were coated with 10μg/ml trimeric spike protein overnight at 4ºC. Serum samples were diluted 1/1000 while lung samples were diluted 1/100. After incubation, the plates were developed using the reagents provided in the Total Ig ELISA kits. Standards for total IgA, IgG1, and IgG2c were used to generate standard curves and calculate the concentration of spike specific antibodies. Plates were read using the Bioteck Synergy H1 hybrid plate reader. Samples were analyzed and graphed using the GraphPad Prism Software. One-way AVOVA was used to determine statistical significance between the groups being compared.

Vaccination and Immune Cell Isolation: Recombinant SARS-CoV-2 proteins were purchased from R&D systems. For vaccination, either 5μg or 2.5μg of the S protein or NC protein (R&D Systems, cat# 10474-CV-050 and cat# 10549-CV-100), both resuspended in PBS, were mixed with 15μl of 1% GC or 15μl of Addavax. Final volume to be delivered intranasal was 20μl, 10μl per nostril delivered to male and female animals in equal numbers. Animals were vaccinated, once, or twice (four weeks apart). Two weeks after the first or second vaccination, the cervical lymph nodes, lungs, serum, and spleen were isolated. Serum was isolated via cardiac puncture and acid-citrate-dextrose (ACD) solution was added to prevent coagulation. The left lobe was used for antibody isolation, while the remaining lobes were used for flow cytometry. Lungs were digested HEPES buffer

containing LiberaseTM 20ug/ml (Roche, cat# 5401127001) and DNase I (100ug/ml) (Roche, cat # 4536282001) for 25 minutes at 37ºC to isolate total leukocytes. Red blood cells were lysed using ACK lysis buffer and then resuspended in RPMI containing 10% FCS and Penicillin/Streptomycin until used for flow cytometry. Spleens and cervical lymph nodes were isolated and enzymatically in digested serum free RPMI containing 100µg/ml Collagenase IV (Gibco, cat# 17104019) and 20µg/ml DNase I (Roche, cat# 4536282001) for 20 minutes at 37ºC. After digestion cells were washed in 1x HBSS, 5% fetal calf serum (FCS), and 5mM EDTA and then for the spleens, the red blood cells were lysed using ACK lysis buffer. The cells were then resuspended in RPMI containing 10% FCS and Penicillin/Streptomycin until used for flow cytometry.

Flow Cytometry: The isolated leukocytes from the lungs, cervical lymph nodes, and spleens were stained with the following antibodies: CD45-BV421 (Biolegend, Cat# 10314), CD40-Pacific Blue (Biolegend, Cat# 124626), Ghost Dye-Violet-510 (Tonbo Biosciences, Cat# 13-0870), CD11b-BV570 (Biolegend, Cat# 101233), CD103-APC (Biolegend , Cat# 121414), CD11c-AF647 (Biolegend, Cat# 117312), MHCII-RedFluor710 (Tonbo Biosciences, Cat# 80-5321), CD86-BV605 (Biolegend, Cat# 105037), Ly6G-SB702 (Invitrogen, Cat# 67-9668-82), Ly6C-BV785 (Biolegend, Cat# 128041), CD64-PE (Biolegend, Cat# 139304), F4/80 PE/Dazzle (Biolegend, Cat# 123146), B220-PE-Cy5 (Biolegend, Cat# 103210), CD19-PE-Cy7 (Invitrogen, Cat# 25-0193-82), CD24-FITC (Biolegend, Cat# 101806), CD44-PerCP-Cy5.5 (Tonbo Biosciences, Cat# 65-0441), CD8-BUV395 (BD Horizon, Cat# 565968), CD3-BUV496 (BD Optibuild, Cat# 741117), CD4-BUV563 (BD Horizon, Cat# 612923), CD62L-BUV737 (BD Horizon, Cat# 612833). Briefly, $5x10^6$ cells were stained with antibodies and placed on ice for 20 minutes in FACs buffer. Cells were washed and then fixed with Fixation Buffer (BD, Cat# 554655) according to manufacturer's instructions. The cells were then washed and resuspended in 1x PBS and then analyzed on the Cytek Aurora spectral flow cytometer. Flow cytometry data was then analyzed using FlowJo software version 10.7 and then graphed using GraphPad Prism. One-way AVOVA was used to determine statistical significance between the groups being compared.

Lung homogenate: At the time of isolation, the left lung lobe was isolated and snap frozen in liquid nitrogen and stored at -80ºC until use. To generate lung homogenate for antibody ELISA, lung tissues were thawed on ice and then resuspended in 0.5ml of T-PER, Tissue Protein Extraction Reagent (ThermoScientific, cat# 78510)

containing Complete Mini Protease Inhibitor Cocktail (Roche, cat# 11836170001). Tissues were homogenized using an electric handheld tissue homogenizer and were stored at -80ºC until used for ELISA.

Viral Challenge: B6.Cg-Tg(K18-ACE2)2Prlmn/J were used for viral challenge experiments. The animals were bred inhouse according to IACUC approved protocols. Male and female mice heterozygous for the K18-hACE2 transgene were used for vaccination and viral challenge experiments. Animals were vaccinated as described above. Briefly, mice were vaccinated twice, four weeks apart. Six weeks after the second vaccination, the animals were challenged with a lethal dose of SARS-CoV-2 (isolate USA-WA1/2020, cat #52281) which was obtained from BEI Resources. The mice were anesthetized with Xylazine/ketamine anesthesia and inoculated intranasally with 2 x 10^4 pfu/mice in 50 ul PBS (25 ul per nostril). Mice were monitored for clinical signs and weight changes every day. Representative mice were sacrificed at day 0 as controls and at days 3 and 5-7 post-infection. The mice that were moribund and or lost >25% body weight were humanely euthanized. The mice that survived the virus challenge were sacrificed on day 22 post-infection. Necropsy on each mouse was performed and tissues were harvested. The left lung was used for virus titer and the right lungs were inflated with 200 ul of 10% formalin for histopathology.

Histopathology Scoring: Lungs from the infected and uninfected mice were infused with 200µl of 10% formalin and placed in a 10% formalin container. Lungs were trimmed, processed, and embedded in paraffin and 5µm sections were cut and stained with hematoxylin and eosin (H&E). The lung sections were scored blindly by two board-certified veterinary pathologists and averages were obtained for each mouse lung. The interstitium, alveoli, bronchioles, and vessels were evaluated for various parameters such as inflammation, edema, fibrin, necrosis, syncytial cells, hemorrhages, ectasia, vasculitis, and thrombi on a scale of 0-4: 0, no lesions; 1, minimal (1 to 10% of lobes affected); 2, mild (10 to 40%); 3, moderate (40-70%); and 4, severe (70 to 100%). The cumulative score from the 24 parameters examined was used for comparison using GraphPad Prism.

Virus Titers: left lung lobes were homogenized in 100 ul serum-free Opti-MEM (Gibco cat# 31985070) using a bead mix (Fisherbrand cat#15340153) in a tissue homogenizer (Fisherbrand cat#15340164). The homogenate was clarified with centrifugation at 2000 rpm x 5 mins. Fifty microliters of supernatant were serially diluted and

100 ul were plated on Vero cells (ATCC cat# CRL1586) monolayer in 12 well plates. The plates were incubated at 37ºC for 1 hr with intermittent gentle shaking every 10 mins. After 1hr post-infection, the media was removed and replaced with post-inoculation media containing overlayed with 0.6% Avicel (Dupont cat# CL-611NF) solution supplemented with 3% FBS (Gibco cat# 10437-28) and 2X MEM (Gibco cat# 11095-080). Three days post-infection overlay was removed, and cells were fixed with 10% neutral buffered formalin for 10-15 mins. The cells were stained with 1% crystal violet solution (Sigma cat# HT90132) and plaques were counted for each dilution. The virus titers were determined by multiplying the number of plaques with the dilution factor.

Acknowledgements

This work was supported in part by Immunophotonics, Inc. The following reagent was deposited by the Centers for Disease Control and Prevention and obtained through BEI Resources, NIAID, and NIH: SARS-Related Coronavirus 2, Isolate USA-WA1/2020, NR-52281.

Disclosure

WRC is co-founder and a member of the Board of Directors of Immunophotonics, Inc. LA, SSKL, and TH declare a conflict of interest as employees with minority ownership stakes of Immunophotonics, Inc., the manufacturer of the proprietary adjuvant GC.

Literature Cited

1. Gaunt, E.R., Harvala, H., McIntyre, C., Templeton, K.E. & Simmonds, P. Disease burden of the most commonly detected respiratory viruses in hospitalized patients calculated using the disability adjusted life year (DALY) model. *J Clin Virol* **52**, 215-221 (2011).

2. Abed, Y. & Boivin, G. Treatment of respiratory virus infections. *Antiviral Res* **70**, 1-16 (2006).

3. Brandtzaeg, P. Function of Mucosa-Associated Lymphoid Tissue in Antibody Formation. *Immunological Investigations* **39**, 303-355 (2010).

4. Holmgren, J. & Czerkinsky, C. Mucosal immunity and vaccines. *Nature Medicine* **11**, S45-S53 (2005).

5. Yusuf, H. & Kett, V. Current prospects and future challenges for nasal vaccine delivery. *Hum Vaccin Immunother* **13**, 34-45 (2017).

6. Lycke, N. Recent progress in mucosal vaccine development: potential and limitations. *Nature Reviews Immunology* **12**, 592-605 (2012).

7. Zhou, S. *et al.* MyD88 is critical for the development of innate and adaptive immunity during acute lymphocytic choriomeningitis virus infection. *Eur J Immunol* **35**, 822-830 (2005).

8. Dubey, V. & MacFadden, D. Disseminated varicella zoster virus infection after vaccination with a live attenuated vaccine. *Canadian Medical Association Journal* **191**, E1025-E1027 (2019).

9. Danziger-Isakov, L., Kumar, D. & Practice, T.A.I.C.o. Vaccination of solid organ transplant candidates and recipients: Guidelines from the American society of transplantation infectious diseases community of practice. *Clinical Transplantation* **33**, e13563 (2019).

10. Sanders, B., Koldijk, M. & Schuitemaker, H. Inactivated Viral Vaccines. *Vaccine Analysis: Strategies, Principles, and Control*, 45-80 (2014).

11. Sumner, R.P., Ren, H., Ferguson, B.J. & Smith, G.L. Increased attenuation but decreased immunogenicity by deletion of multiple vaccinia virus immunomodulators. *Vaccine* **34**, 4827-4834 (2016).

12. Moyle, P.M. & Toth, I. Modern Subunit Vaccines: Development, Components, and Research Opportunities. *ChemMedChem* **8**, 360-376 (2013).

13. Pulendran, B. & Ahmed, R. Immunological mechanisms of vaccination. *Nat Immunol* **12**, 509-517 (2011).

14. Pulendran, B., S. Arunachalam, P. & O'Hagan, D.T. Emerging concepts in the science of vaccine adjuvants. *Nature Reviews Drug Discovery* (2021).

15. Wang, Z.-B. & Xu, J. Better Adjuvants for Better Vaccines: Progress in Adjuvant Delivery Systems, Modifications, and Adjuvant-Antigen Codelivery. *Vaccines (Basel)* **8**, 128 (2020).

16. McGhee, J.R. & Fujihashi, K. Inside the Mucosal Immune System. *PLOS Biology* **10**, e1001397 (2012).

17. Freytag, L.C. & Clements, J.D. Chapter 61 - Mucosal Adjuvants: New Developments and Challenges. In: Mestecky, J. *et al.* (eds). *Mucosal Immunology (Fourth Edition)*. Academic Press: Boston, 2015, pp 1183-1199.

18. Li, S. *et al.* Type I Interferons: Distinct Biological Activities and Current Applications for Viral Infection. *Cellular Physiology and Biochemistry* **51**, 2377-2396 (2018).

19. Su, F., Patel, G.B., Hu, S. & Chen, W. Induction of mucosal immunity through systemic immunization: Phantom or reality? *Hum Vaccin Immunother* **12**, 1070-1079 (2016).

20. Vassilieva, E.V., Taylor, D.W. & Compans, R.W. Combination of STING Pathway Agonist With Saponin Is an Effective Adjuvant in Immunosenescent Mice. *Frontiers in Immunology* **10** (2019).

21. Van Dis, E. *et al.* STING-Activating Adjuvants Elicit a Th17 Immune Response and Protect against Mycobacterium tuberculosis Infection. *Cell Rep* **23**, 1435-1447 (2018).

22. Wang, H. *et al.* cGAS is essential for the antitumor effect of immune checkpoint blockade. *Proceedings of the National Academy of Sciences of the United States of America* **114**, 1637-1642 (2017).

23. Osorio, F. & e Sousa, C.R. Myeloid C-type lectin receptors in pathogen recognition and host defense. *Immunity* **34**, 651-664 (2011).

24. Zaharoff, D.A., Rogers, C.J., Hance, K.W., Schlom, J. & Greiner, J.W. Chitosan solution enhances both humoral and cell-mediated immune responses to subcutaneous vaccination. *Vaccine* **25**, 2085-2094 (2007).

25. Carroll, E.C. *et al.* The vaccine adjuvant chitosan promotes cellular immunity via DNA sensor cGAS-STING-dependent induction of type I interferons. *Immunity* **44**, 597-608 (2016).

26. Hoover, A.R. *et al.* A novel biopolymer synergizes type I IFN and IL-1β production through STING. *bioRxiv*, 2022.2007.2022.501157 (2022).

27. Li, X. *et al.* Chitin, Chitosan, and Glycated Chitosan Regulate Immune Responses: The Novel Adjuvants for Cancer Vaccine. *Clinical and Developmental Immunology* **2013**, 387023 (2013).

28. Zhao, D. *et al.* Biomedical Applications of Chitosan and Its Derivative Nanoparticles. *Polymers (Basel)* **10**, 462 (2018).

29. Bellich, B., D'Agostino, I., Semeraro, S., Gamini, A. & Cesàro, A. "The Good, the Bad and the Ugly" of Chitosans. *Marine Drugs* **14**, 99 (2016).

30. Li, X. *et al.* Preliminary safety and efficacy results of laser immunotherapy for the treatment of metastatic breast cancer patients. *Photochem Photobiol Sci* **10**, 817-821 (2011).

31. Liu, K. *et al.* Antigen presentation and interferon signatures in B cells driven by localized ablative cancer immunotherapy correlate with extended survival. *Theranostics* **12**, 639-656 (2022).

32. Korbelik, M., Hode, T., Lam, S.S. & Chen, W.R. Novel Immune Stimulant Amplifies Direct Tumoricidal Effect of Cancer Ablation Therapies and Their Systemic Antitumor Immune Efficacy. *Cells* **10**, 492 (2021).

33. Barchfeld, G.L. *et al.* The adjuvants MF59 and LT-K63 enhance the mucosal and systemic immunogenicity of subunit influenza vaccine administered intranasally in mice. *Vaccine* **17**, 695-704 (1999).

34. Lavelle, E.C. & Ward, R.W. Mucosal vaccines — fortifying the frontiers. *Nature Reviews Immunology* **22**, 236-250 (2022).

35. Reed, S.G., Orr, M.T. & Fox, C.B. Key roles of adjuvants in modern vaccines. *Nature Medicine* **19**, 1597-1608 (2013).

36. Stetson, D.B. & Medzhitov, R. Type I interferons in host defense. *Immunity* **25**, 373-381 (2006).

37. Fink, K. *et al.* Early type interferon-mediated signals on B cells specifically enhance antiviral humoral responses. *Eur J Immunol* **36**, 2094-2105 (2006).

38. Kolumam, G.A., Thomas, S., Thompson, L.J., Sprent, J. & Murali-Krishna, K. Type I interferons act directly on CD8 T cells to allow clonal expansion and memory formation in response to viral infection. *The Journal of experimental medicine* **202**, 637-650 (2005).

39. Kuo, T.-Y. *et al.* Development of CpG-adjuvanted stable prefusion SARS-CoV-2 spike antigen as a subunit vaccine against COVID-19. *Scientific Reports* **10**, 20085 (2020).

40. Campbell, J.D. Development of the CpG Adjuvant 1018: A Case Study. *Methods in molecular biology (Clifton, N.J.)* **1494**, 15-27 (2017).

41. Hoover, A.R. *et al.* ScRNA-seq reveals tumor microenvironment remodeling induced by local intervention-based immunotherapy. *bioRxiv*, 2020.2010.2002.323006 (2020).

42. Sallusto, F. & Lanzavecchia, A. The instructive role of dendritic cells on T-cell responses. *Arthritis Res* **4 Suppl 3**, S127-S132 (2002).

43. Hoover, A.R. *et al.* Single-cell RNA sequencing reveals localized tumour ablation and intratumoural immunostimulant delivery potentiate T cell mediated tumour killing. *Clinical and Translational Medicine* **12**, e937 (2022).

44. Zhou, F. *et al.* Local phototherapy synergizes with immunoadjuvant for treatment of pancreatic cancer through induced immunogenic tumor vaccine. *Clin. Cancer Res.* **24**, 5335-5346 (2018).

45. El-Hussein, A., Lam, S.S., Raker, J., Chen, W.R. & Hamblin, M.R. N-Dihydrogalactochitosan as a potent immune activator for dendritic cells. *Journal of Biomedical Materials Research Part A* (2016).

46. Curtsinger, J.M., Valenzuela, J.O., Agarwal, P., Lins, D. & Mescher, M.F. Cutting Edge: Type I IFNs Provide a Third Signal to CD8 T Cells to Stimulate Clonal Expansion and Differentiation. *The Journal of Immunology* **174**, 4465-4469 (2005).

47. Ben-Sasson, S.Z., Wang, K., Cohen, J. & Paul, W.E. IL-1β strikingly enhances antigen-driven CD4 and CD8 T-cell responses. *Cold Spring Harbor symposia on quantitative biology* **78**, 117-124 (2013).

48. Oliveira, S.C., de Magalhães, M.T.Q. & Homan, E.J. Immunoinformatic Analysis of SARS-CoV-2 Nucleocapsid Protein and Identification of COVID-19 Vaccine Targets. *Frontiers in Immunology* **11** (2020).

49. Smits, V.A.J. *et al.* The Nucleocapsid protein triggers the main humoral immune response in COVID-19 patients. *Biochemical and Biophysical Research Communications* **543**, 45-49 (2021).

50. Lee, E. *et al.* Identification of SARS-CoV-2 Nucleocapsid and Spike T-Cell Epitopes for Assessing T-Cell Immunity. *J Virol* **95** (2021).

51. Lineburg, K.E. *et al.* CD8(+) T cells specific for an immunodominant SARS-CoV-2 nucleocapsid epitope cross-react with selective seasonal coronaviruses. *Immunity* **54**, 1055-1065.e1055 (2021).

52. Carotti, M. *et al.* Chest CT features of coronavirus disease 2019 (COVID-19) pneumonia: key points for radiologists. *La radiologia medica* **125**, 636-646 (2020).

53. Tsang, K.W. & Bilton, D. Clinical challenges in managing bronchiectasis. *Respirology* **14**, 637-650 (2009).

54. Ambrosetti, M.C. *et al.* Rapid onset of bronchiectasis in COVID-19 Pneumonia: two cases studied with CT. *Radiol Case Rep* **15**, 2098-2103 (2020).

55. McCray, P.B., Jr. *et al.* Lethal infection of K18-hACE2 mice infected with severe acute respiratory syndrome coronavirus. *J Virol* **81**, 813-821 (2007).

Figure 1. N-dihydrogalactochitosan retains antigen at the site of injection and stimulates a variety of antiviral pathways.

A. Retention of antigen by GC. GC (1%) was mixed with Texas-Red labeled ovalbumin (OVA-TR) and injected intradermally into the flank of C57BL/6 mice. Whole body fluorescent imaging was performed over a period of several days. The percentage rate of change was calculated to quantify the amount of OVA localized to the injection site. Two-way ANOVA was used for statistical analysis.

B. Stimulation of antiviral response pathways by GC. Wild type BMDCs were stimulated +/- GC for 24 hours prior to harvesting for bulk RNA-sequencing analysis. KEGG Pathways Analysis revealed that GC stimulated a variety of antiviral response pathways.

C. Heatmap showing the expression of various pattern recognition receptors (PRRs) in PBS and GC stimulated BMDCs (n=3).

Figure 2. Multiple intranasal vaccinations using GC with recombinant SARS-CoV-2 spike protein drives localized, systemic antigen-specific humoral responses, in comparison with the adjuvant MF-59 equivalent, Addavax (AV).

A. Schematic of the intranasal (I.N.) vaccination (2X) strategy and analysis using GC or AV as the adjuvant.

B. Total IgA and S-specific IgA from left lung lobe homogenates harvested 2 weeks after the 2nd vaccination. One-way ANOVA was used for statistical analysis.

C. Total serum IgG1 and S-specific IgG1 levels 1 week after the 1st vaccination, 1 week after the 2nd vaccination, and 2 weeks after the 2nd vaccination.

D. Total serum IgG2c and S-specific IgG2c levels 1 week after the 1st vaccination, 1 week after the 2nd vaccination, and 2 weeks after the 2nd vaccination.

Figure 3. Intranasal administration of GC with recombinant SARS-CoV-2 spike protein increases cervical lymph node cellularity.

A-C. Activation of leukocytes after two-dose vaccination. Cervical lymph nodes were isolated two weeks after the 2nd intranasal vaccination and analyzed via flow cytometry.

A. Activation of $CD8^+$ T cells after two-dose vaccination. $CD8^+$ T cells were gated on Live, $CD45^+CD3^+CD8^+$ cells prior to analysis with CD44 and CD62L. Total cellularity of CD8 T cells, $CD8^+CD44^+$, $CD8^+CD44^+CD62L^+$, and $CD8^+CD62L^+$ was calculated. One-way ANOVA was used for statistical analysis.

B. Activation of $CD4^+$ T cells after two-dose vaccination. $CD4^+$ T cells were gated on Live, $CD45^+CD3^+CD4^+$ cells prior to analysis with CD44 and CD62L. Total cellularity of CD4 T cells, $CD4^+CD44^+$, $CD4^+CD44^+CD62L^+$, and $CD4^+CD62L^+$ was calculated. One-way ANOVA was used for statistical analysis.

C. Activation of B cells after two-dose vaccination. B cells were gated on Live, $CD45^+CD19^+B220^+$ cells and then calculated for total cellularity. One-way ANOVA was used for statistical analysis.

Figure 4. Combining recombinant SARS-CoV-2 spike and nucleocapsid proteins for intranasal vaccination enhances humoral and cellular responses.

A. Total Serum IgG1 and S-specific IgG1 levels 2 weeks after the 2nd vaccination. One-way ANOVA was used for statistical analysis.

B. Total Serum IgG2c and S-specific IgG2c levels 2 weeks after the 2nd vaccination. One-way ANOVA was used for statistical analysis.

C. Total IgA and S-specific IgA from left lung lobe homogenates harvested 2 weeks after 2nd vaccination. One-way ANOVA was used for statistical analysis.

D-E. T cell activation by GC with recombinant proteins. Cervical lymph nodes were isolated two weeks after the 2nd intranasal vaccination and analyzed via flow cytometry.

D. $CD4^+$ T cells were gated on Live, $CD45^+CD3^+CD4^+$ cells prior to analysis with CD44 and CD62L. Total cellularity of CD4 T cells, $CD4^+CD44^+$, $CD4^+CD44^+CD62L^+$, and $CD4^+CD62L^+$ was calculated. One-way ANOVA was used for statistical analysis.

E. $CD8^+$ T cells were gated on Live, $CD45^+CD3^+CD8^+$ cells prior to analysis with CD44 and CD62L. Total cellularity of CD8 T cells, $CD8^+CD44^+$, $CD8^+CD44^+CD62L^+$, and $CD8^+CD62L^+$ was calculated. One-way ANOVA was used for statistical analysis.

Figure 5. Intranasal vaccination with GC and recombinant SARS-CoV-2 spike and nucleocapsid proteins protects mice against lethal viral challenge.

A. Schematic of the vaccination and viral challenge strategy for K18-hACE-2 animals.

B. Survival rates of animals challenged by SARS-CoV-2 virus over a course of 21 days (n=15-24).

C. Percent body weight change over a period of 21 days in virally infected animals.

D. Plaque assays performed in lung homogenates on day 5 post viral infection (n=3 per group). Data represents mean ± SE of the respective groups. One-way ANOVA was used for statistical analysis.

Figure 6. Intranasal vaccination with GC and recombinant SARS-CoV-2 spike and nucleocapsid proteins protects mice against severe lung pathology.

A-D. 10x H&E sections of lungs at days 0, 3, 6, and 21 post SARS-CoV-2 challenge (n=15-24 per group).

A. Day 0: H&E-stained lungs demonstrating normal lung architecture.

B. Day 3: Interstitial (arrow) and peribronchial and perivascular immune infiltration (open circles) post infection.

C. Day 6: Bronchiectasia (arrowheads) and bronchioles infiltrated with mucus and immune cells (arrows) post infection. Immune infiltration was also observed in the alveoli (empty arrowhead). Hemorrhages in the alveolar spaces (*) and peribronchial and perivascular immune infiltration (open circles) were observed.

D. Day 21: Peribronchial and perivascular immune infiltration (open circles) post infection.

E-I. Pathological evaluation and scoring for the lung sections at days 0, 3, 5, 6/7/8, and 21 post infection. The interstitium, alveoli, bronchioles, and vessels were evaluated for various parameters such as inflammation, edema, fibrin, necrosis, syncytial cells, hemorrhages, ectasia, vasculitis, and thrombi on a scale of 0-4: 0, no lesions; 1, minimal (1 to 10% of lobes affected); 2, mild (10 to 40%); 3, moderate (40-70%); and 4, severe (70 to 100%). The cumulative score was obtained from the 24 parameters examined.

E. Cumulative histopathology scores for day 0. One-way ANOVA was used for statistical analysis.

F. Cumulative histopathology scores for day 3. One-way ANOVA was used for statistical analysis.

G. Cumulative histopathology scores for day 5. One-way ANOVA was used for statistical analysis.

H. Cumulative histopathology scores for day 6/7/8 at the point of euthanasia. One-way ANOVA was used for statistical analysis.

I. Cumulative histopathology scores for day 21. One-way ANOVA was used for statistical analysis.

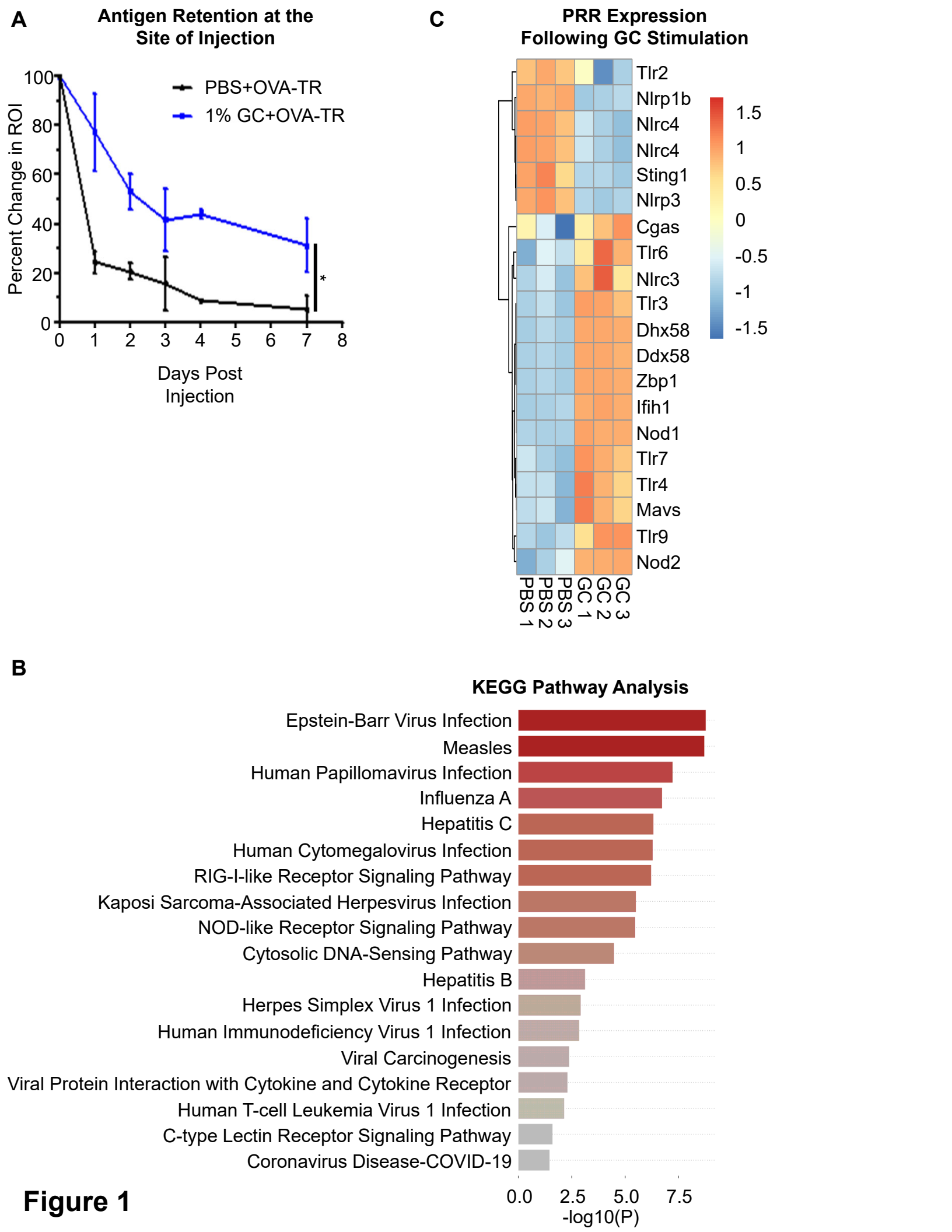
A
Antigen Retention at the Site of Injection
PBS+OVA-TR
1% GC+OVA-TR
Percent Change in ROI
Days Post Injection
*
C
PRR Expression Following GC Stimulation
Tlr2
Nlrp1b
Nlrc4
Nlrc4
Sting1
Nlrp3
Cgas
Tlr6
Nlrc3
Tlr3
Dhx58
Ddx58
Zbp1
Ifih1
Nod1
Tlr7
Tlr4
Mavs
Tlr9
Nod2
PBS 1
PBS 2
PBS 3
GC 1
GC 2
GC 3
B
KEGG Pathway Analysis
Epstein-Barr Virus Infection
Measles
Human Papillomavirus Infection
Influenza A
Hepatitis C
Human Cytomegalovirus Infection
RIG-I-like Receptor Signaling Pathway
Kaposi Sarcoma-Associated Herpesvirus Infection
NOD-like Receptor Signaling Pathway
Cytosolic DNA-Sensing Pathway
Hepatitis B
Herpes Simplex Virus 1 Infection
Human Immunodeficiency Virus 1 Infection
Viral Carcinogenesis
Viral Protein Interaction with Cytokine and Cytokine Receptor
Human T-cell Leukemia Virus 1 Infection
C-type Lectin Receptor Signaling Pathway
Coronavirus Disease-COVID-19
-log10(P)

Figure 1

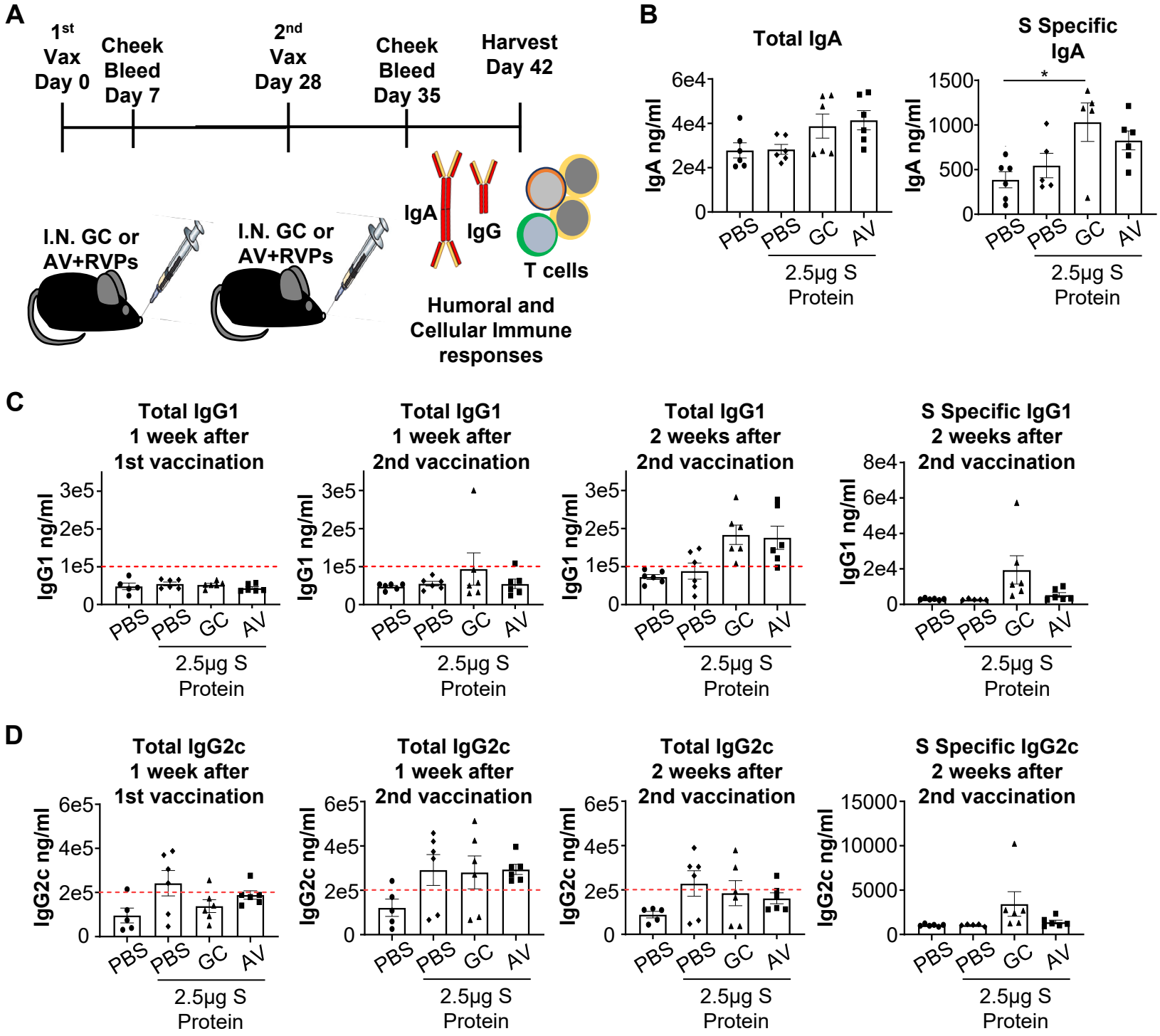
A
1st Vax Day 0
Cheek Bleed Day 7
2nd Vax Day 28
Cheek Bleed Day 35
Harvest Day 42
I.N. GC or AV+RVPs
I.N. GC or AV+RVPs
IgA
IgG
T cells
Humoral and Cellular Immune responses
B
Total IgA
IgA ng/ml
6e4
4e4
2e4
0
PBS
PBS
GC
AV
2.5µg S Protein
S Specific IgA
IgA ng/ml
1500
1000
500
0
*
PBS
PBS
GC
AV
2.5µg S Protein
C
Total IgG1 1 week after 1st vaccination
Total IgG1 1 week after 2nd vaccination
Total IgG1 2 weeks after 2nd vaccination
S Specific IgG1 2 weeks after 2nd vaccination
IgG1 ng/ml
3e5
2e5
1e5
0
8e4
6e4
4e4
2e4
PBS
PBS
GC
AV
2.5µg S Protein
D
Total IgG2c 1 week after 1st vaccination
Total IgG2c 1 week after 2nd vaccination
Total IgG2c 2 weeks after 2nd vaccination
S Specific IgG2c 2 weeks after 2nd vaccination
IgG2c ng/ml
6e5
4e5
2e5
0
15000
10000
5000
PBS
PBS
GC
AV
2.5µg S Protein

Figure 2

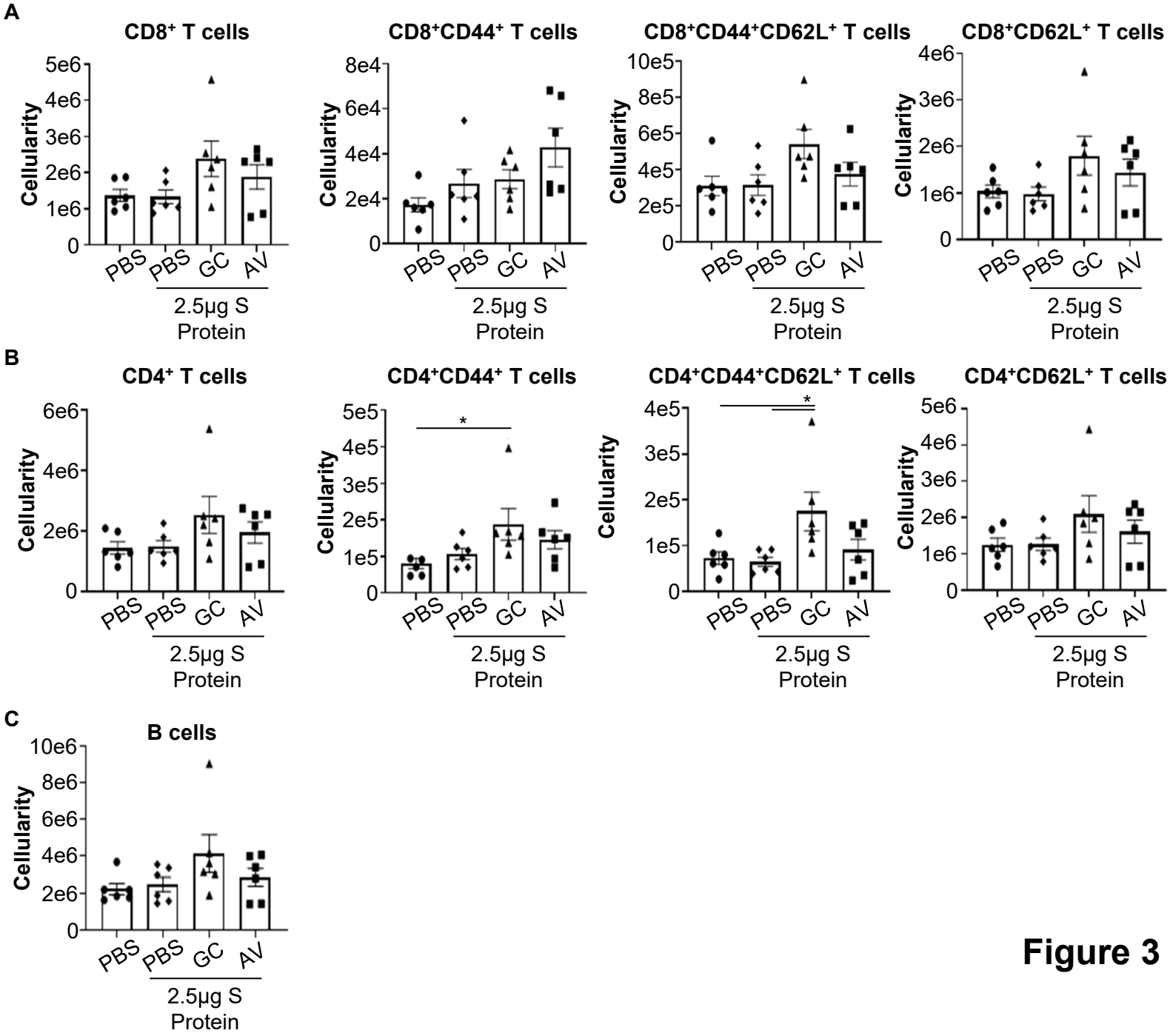
A
CD8+ T cells
CD8+CD44+ T cells
CD8+CD44+CD62L+ T cells
CD8+CD62L+ T cells
Cellularity
PBS
PBS
GC
AV
2.5µg S Protein
B
CD4+ T cells
CD4+CD44+ T cells
CD4+CD44+CD62L+ T cells
CD4+CD62L+ T cells
*
C
B cells

Figure 3

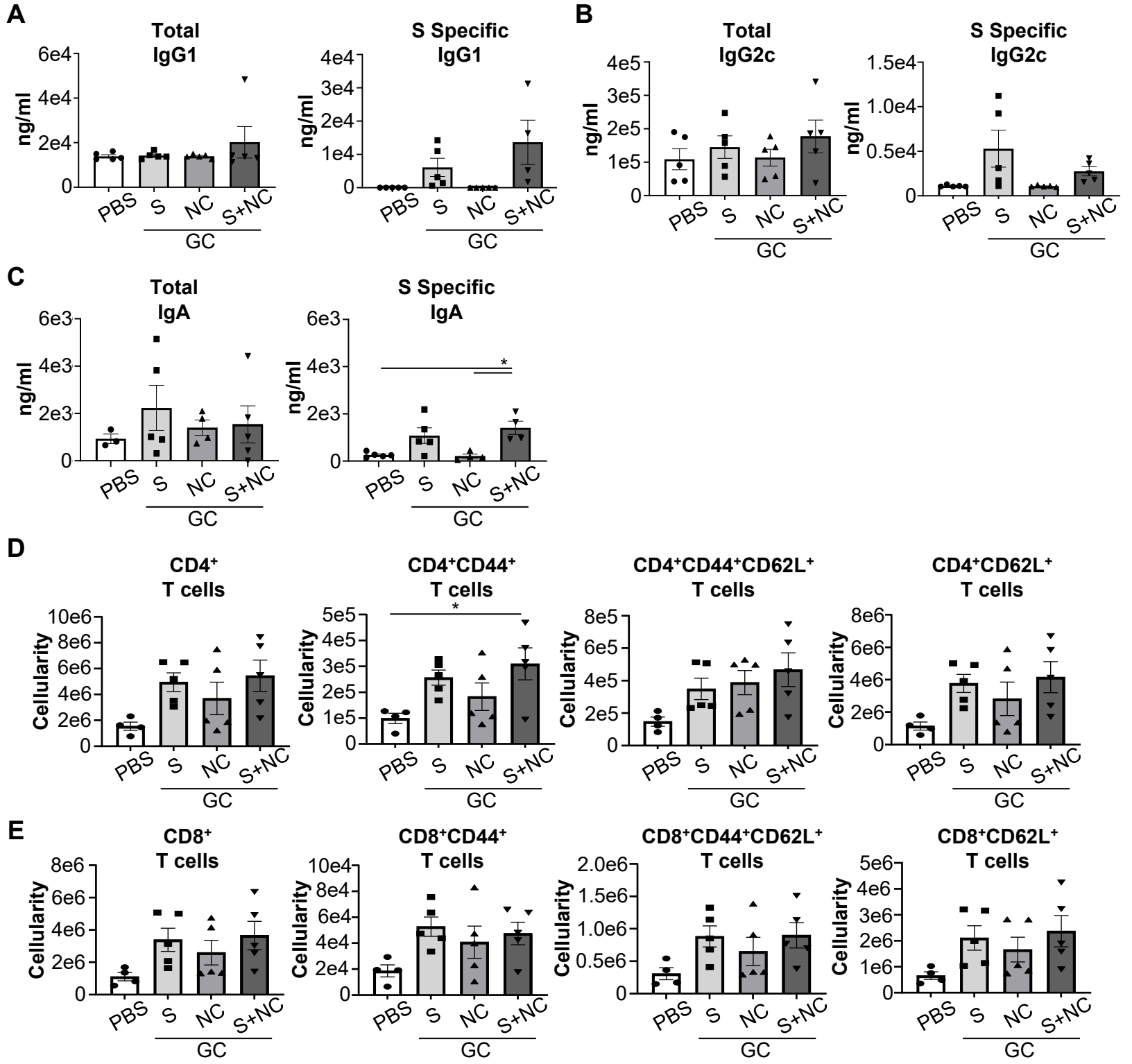
A
Total IgG1
S Specific IgG1
ng/ml
PBS
S
NC
S+NC
GC
B
Total IgG2c
S Specific IgG2c
C
Total IgA
S Specific IgA
*
D
CD4+ T cells
CD4+CD44+ T cells
CD4+CD44+CD62L+ T cells
CD4+CD62L+ T cells
Cellularity
E
CD8+ T cells
CD8+CD44+ T cells
CD8+CD44+CD62L+ T cells
CD8+CD62L+ T cells

Figure 4

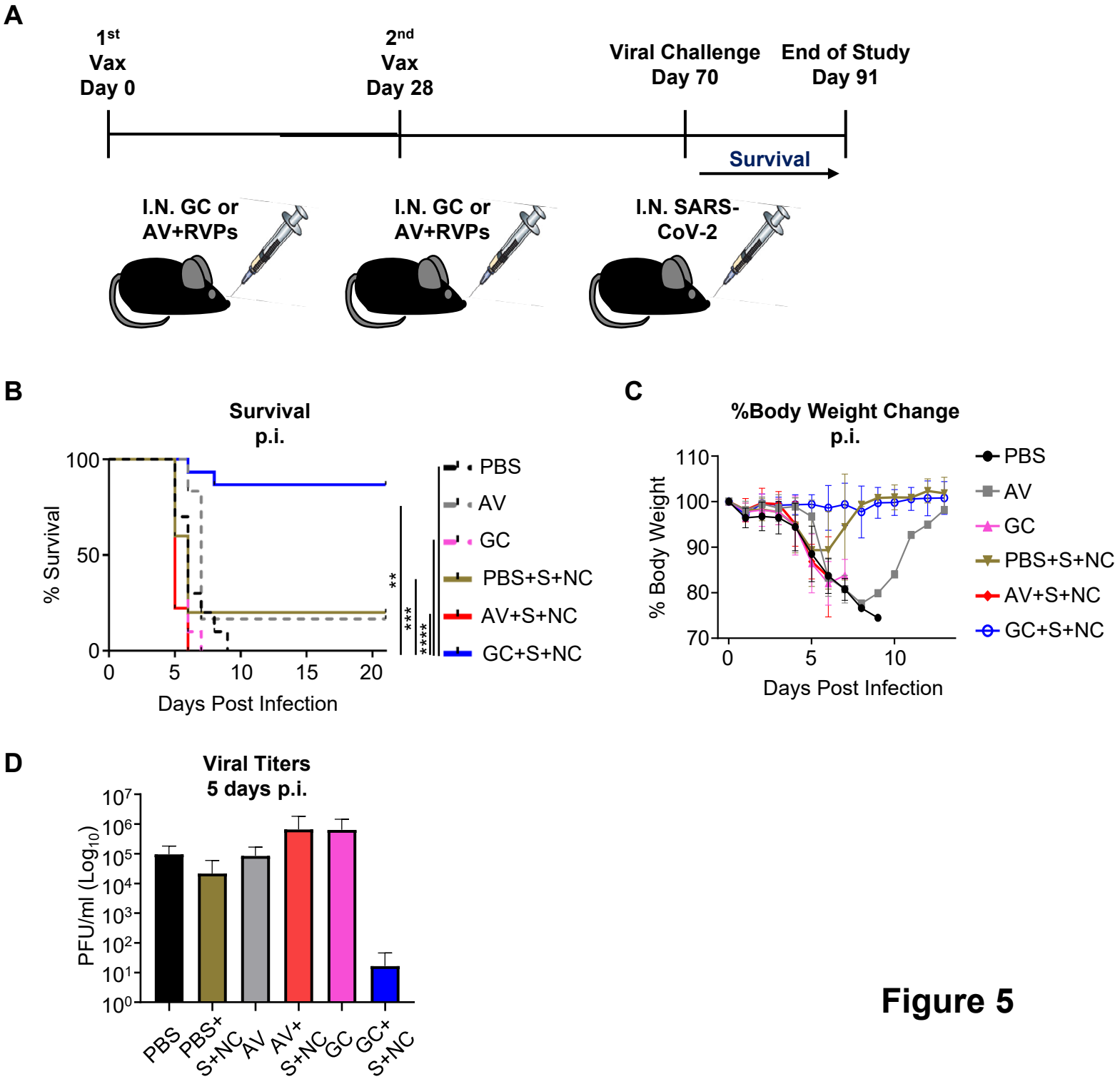
A
1st Vax Day 0
2nd Vax Day 28
Viral Challenge Day 70
End of Study Day 91
Survival
I.N. GC or AV+RVPs
I.N. GC or AV+RVPs
I.N. SARS-CoV-2
B
Survival p.i.
% Survival
Days Post Infection
PBS
AV
GC
PBS+S+NC
AV+S+NC
GC+S+NC
C
%Body Weight Change p.i.
% Body Weight
Days Post Infection
D
Viral Titers 5 days p.i.
PFU/ml (Log10)
PBS
PBS+ S+NC
AV
AV+ S+NC
GC
GC+ S+NC

Figure 5

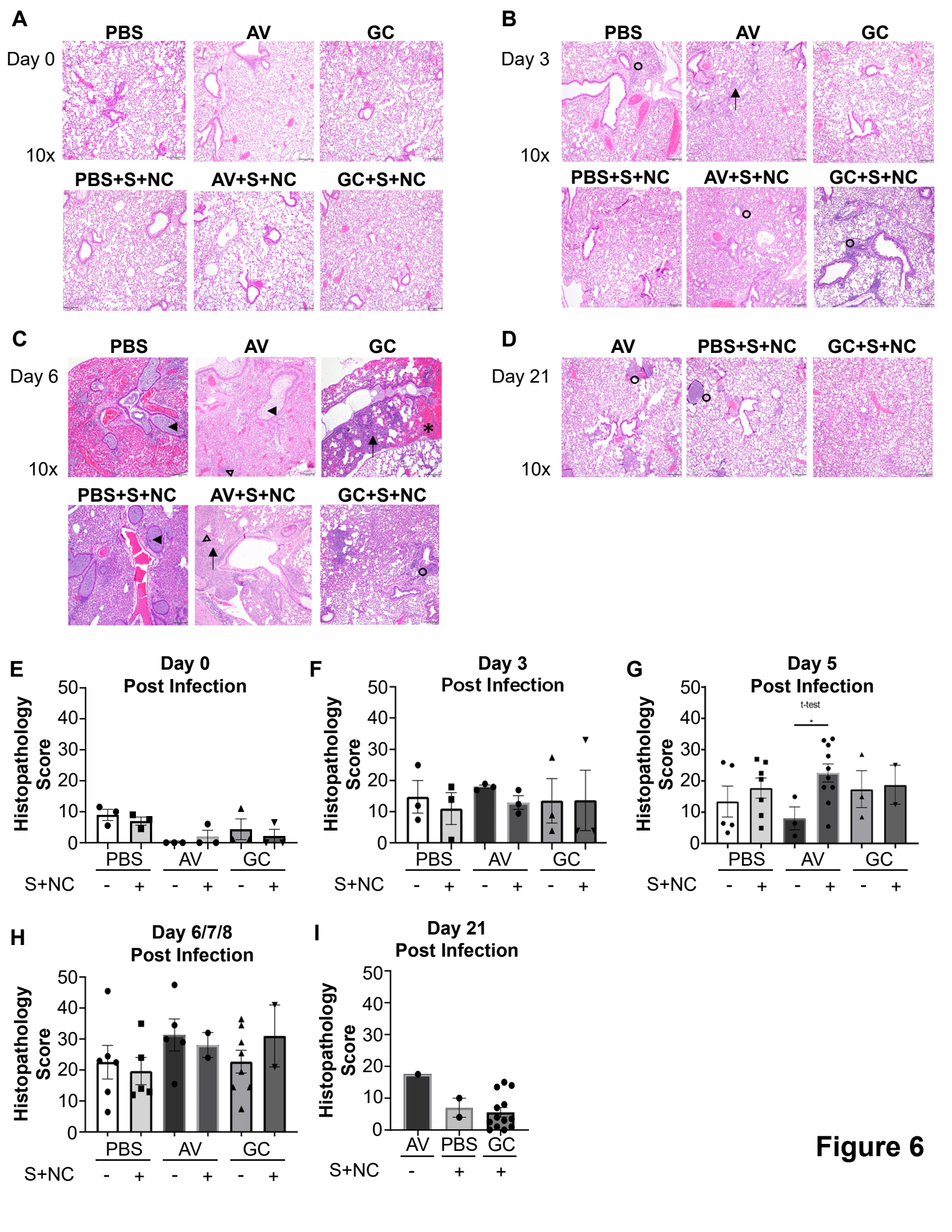
A
PBS
AV
GC
Day 0
10x
PBS+S+NC
AV+S+NC
GC+S+NC
B
PBS
AV
GC
Day 3
10x
PBS+S+NC
AV+S+NC
GC+S+NC
C
PBS
AV
GC
Day 6
10x
PBS+S+NC
AV+S+NC
GC+S+NC
D
AV
PBS+S+NC
GC+S+NC
Day 21
10x
E
Day 0
Post Infection
Histopathology Score
PBS
AV
GC
S+NC
F
Day 3
Post Infection
Histopathology Score
PBS
AV
GC
S+NC
G
Day 5
Post Infection
t-test
Histopathology Score
PBS
AV
GC
S+NC
H
Day 6/7/8
Post Infection
Histopathology Score
PBS
AV
GC
S+NC
I
Day 21
Post Infection
Histopathology Score
AV
PBS
GC
S+NC

Figure 6